inorganics

MDPI

Article

Hyperthermia and Photocatalytic Performance of Magnetic Polyvinyl Alcohol under External Magnetic Field

Manal M. Khowdiary [1], Hind Alsnani [2] and Mohamed S. A. Darwish [3,*]

[1] Department of Chemistry, Al-Leith University College, Umm Al Qura University, Makkah 2207, Saudi Arabia; mmkhowdiary@uqu.edu.sa
[2] Department of Physics, Al-Leith University College, Umm Al Qura University, Makkah 220, Saudi Arabia; hasnani@uqu.edu.sa
[3] Egyptian Petroleum Research Institute, 1 Ahmed El-Zomor Street, El Zohour Region, Nasr City, Cairo 11727, Egypt
* Correspondence: msa.darwish@gmail.com

Abstract: The promising physical and chemical properties of components of magnetic polymers could enable extending their intelligent behaviors to material applications. Indeed, investigation into magnetic nanofillers to ensure their uniform dispersion within the polymer matrix remains a great challenge at present. In this work, polyvinyl alcohol-stabilized iron oxide nanoparticles (PVA@IONPs) were prepared using ultrasonic-assisted coprecipitation at room temperature. It is possible to produce PVA@IONPs with desirable shapes and sizes, which would enable the control of their hyperthermia and photocatalytic performance under an external magnetic field. The saturation magnetization of PVA@IONPs (45.08 emu g^{-1}) was enhanced to the level of IONPs (41.93 emu g^{-1}). The PVA@IONPs showed good photocatalytic and outstanding self-heating behavior. The hydrogen yield was 60 mmole min^{-1} g^{-1} for photocatalyst PVA@IONPs under visible light with magnetic force. In addition, the PVA@IONPs exhibited a higher specific absorption rate (SAR) than IONPs under the same magnetic field conditions. The PVA@IONPs displayed superior self-heating and photocatalytic performances, rendering them appropriate materials for biomedical and environmental applications.

Keywords: hyperthermia; PVA@IONPs; specific absorption rate; photocatalytic properties

Citation: Khowdiary, M.M.; Alsnani, H.; Darwish, M.S.A. Hyperthermia and Photocatalytic Performance of Magnetic Polyvinyl Alcohol under External Magnetic Field. *Inorganics* **2024**, *12*, 47. https://doi.org/10.3390/inorganics12020047

Academic Editor: Li Wang

Received: 2 January 2024
Revised: 28 January 2024
Accepted: 29 January 2024
Published: 30 January 2024

1. Introduction

Magnetic polymers have excellent prospects for different applications as the incorporation of the matrix displays behavior that none of its ingredient structures separately have [1–3]. It can be synthesized in the form of stimuli-responsive polymeric nanoparticles with desirable shapes and sizes, which enables the control of their magnetic and optical properties [4–6]. Naked magnetic nanoparticles show a high surface area and magnetic dipole–dipole force, which leads to agglomerated particle formulation [7,8]. The aggregation of particles tends towards a magnetic property due to the lack of the size-dependent behavior in the particles. Magnetic material has been utilized in several applications, such as biomedical, environmental, and industrial applications [9–16]. Magnetic nanoparticles with modified/functionalized surfaces could result in an improved dispersion of nanoparticles into the polymer matrix. The surface modification/functionalization of magnetic nanoparticles improves the interfacial reaction and compatibility between both nanofillers and the polymer matrix. The functionalization of magnetic nanoparticles depends on introducing an organic or polymer coating via chemical/physical reactions to enhance their compatibility, leading to improved dispersion and the ability to fabricate stimuli-responsive polymeric nanoparticles for advanced applications. The introduction of a polyvinyl alcohol (PVA) layer on the surface of iron oxide nanoparticles (IONPs) can shield the magnetic iron oxide core from oxidation by the harsh chemical environment or physiological body fluid, enhancing the colloidal stability of the nanoparticles via electrostatic repulsions

and steric influences and their compatibility in a physiological environment. PVA with emulsifying and adhesive properties enables the preparation of hydrogel structures and can bind to antibodies, proteins, enzymes, or drugs. PVA with dense electrons of free lone pairs can strongly affect the photo behavior by absorbing light irradiation and instantly being excited by the influence of irradiation. Several techniques have been applied for the preparation of polymeric PVA@IONPs, such as the electrospinning method and ex situ, in situ, and solution-mixing techniques [17–27]. Hence, this work aimed to prepare polyvinyl alcohol-stabilized iron oxide nanoparticles (PVA@IONPs) via ultrasonic-assisted coprecipitation at room temperature. The nanoparticles were prepared via an environmentally friendly process (without surfactant or organic solvent) and a simple technique (at room temperature with non-expensive materials). The prepared nanoparticles displayed superior self-heating and photocatalytic performances. Iron oxide nanoparticles show magnetic stimulation heating, which could be used in the biomedical field and catalytic applications. The stimulation efficiency depends on the IONPs' behavior and the magnetic field conditions. The nanoparticles' size affects their magnetic domains and magneto-static energy. The nanoparticle's size affects its magnetic domains and magneto-static energy. The transformation of magnetic power into thermal power in IONPs has shown notable potential as a hyperthermia cancer treatment in biomedical applications [13,14]. The photocatalytic activity is mainly dependent on the electronic structure of the catalyst and its magnetic properties. Magnetic field-enhanced photocatalysis fundamentally operates via three mechanisms: spin polarization, the Lorentz force, and the magneto-resistance effect. A spin polarization increase in photocatalysis is attributed to a magnetic field acting on the spin–orbit coupling in the photocatalyst, in this way regulating the spin polarization to set the photo-generated charge carrier and surface reaction performance. Improving photocatalysis via the Lorentz force and magneto-resistance effect is related to the promotion of the separation and transfer of photo-generated charge carriers [9]. In this work, the photocatalytic and self-heating performances of polymeric PVA@IONPs were evaluated. The polymeric PVA@IONPs were fabricated via an ultrasonic-assisted coprecipitation technique at room temperature. The properties of the prepared magnetic materials were investigated with XRD, VSM, TEM, zeta potential, ICP-OES, and UV–vis spectroscopy. In addition, the hyperthermia performance and photocatalytic activity were evaluated.

2. Results and Discussion

2.1. Characterization of Nanoparticles

The influence of coating IONPs with a PVA layer via an ultrasonic-assisted coprecipitation technique on the nanoparticle's behaviors was studied. The particle sizes of the fabricated nanoparticles were investigated by TEM (Figure 1). IONPs and PVA@IONPs exhibited an almost spherical morphology with a wide size distribution of 13 ± 3 and 16 ± 4 nm, respectively. The corresponding selected area electron diffraction (SAED) image of nanoparticles displays ring characteristics consistent with a structure composed of small domains, with their crystallographic axes randomly oriented from another. The SAED pattern shows diffuse rings with less intensity that can be indexed to the nanoparticle's plane reflections. The detected aggregated IONPs are due to the high surface energy and the dipole–dipole effect [28]. The absence of a covering shell and aerobic surroundings supported the interaction. The nanoparticles become agglomerated into large groups and increase the size distribution. The aggregation is minimized by inserting a covering polymer shell. The shell acts as a protecting layer to set and control the particle size [29]. The PVA@IONPs showed a lower aggregation attitude than the IONPs. The PVA layer on the surface of the IONPs led to improved dispersion properties. The PVA shell enhanced the advantage of increasing the repulsion to balance the magnetic and Van der Waals forces. The improved dispersion of the PVA@IONPs is expected to affect the nanoparticles' magneto-photo-efficiency. The elemental content for the PVA@IONPs was recorded using TEM-EDAX (Figure 1). We observed distinctive bands at 6.5 and 0.6 keV related to the presence of iron, which proves IONP fabrication. PVA existence was detected by the band

for C at 0.2 keV and for O and 0.5 keV. The presence of PVA and Fe in the PVA@IONPs was confirmed by TEM-EDAX. The mass percentage of iron in the IONPs was measured at 50.8 using ICP-OES. The mass percentage of iron in the PVA@IONPs was 66.6%, which is expected to impact their heating and photocatalytic performance.

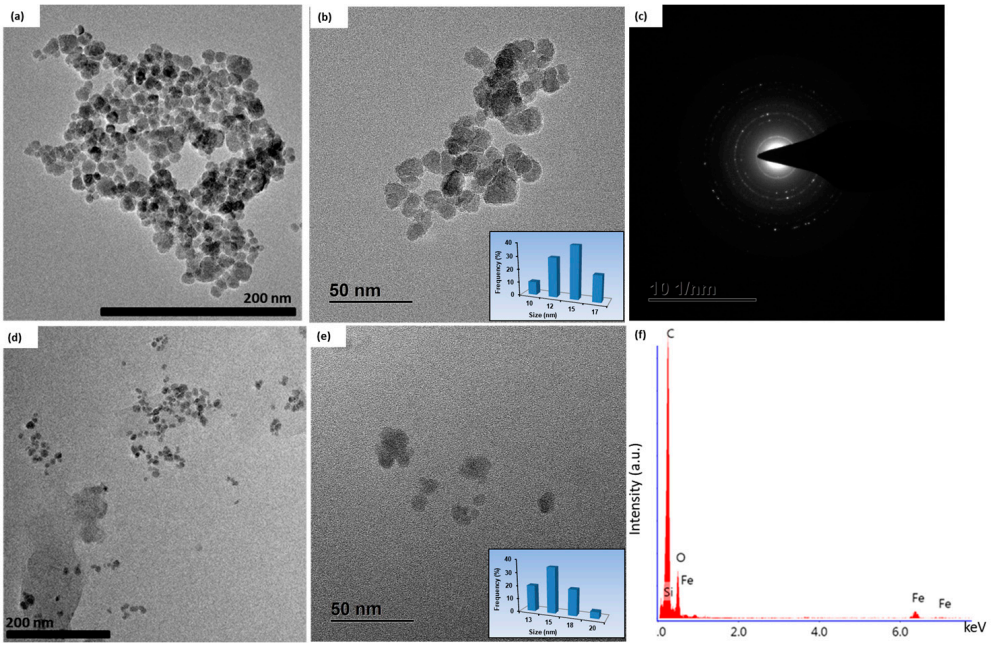

Figure 1. (**a**–**c**) TEM-SAED of IONPs and (**d**–**f**) TEM-EDAX of PVA@IONPs.

The phase of iron oxide was studied using XRD. The peaks (220), (311), (400), (422), (511), and (440) confirm the standard pattern (reference code: 98-015-8742) for the dominant Fe_3O_4. However, the peaks (024), (116), (113), and (104) confirm α-Fe_2O_3 (Figure 2) [30]. Under an atmospheric state with a shortage of encapsulated oxygen, the Fe_3O_4 phase could oxidize, i.e., $Fe_3O_4 \rightarrow Fe_2O_3$. The indexed peaks (220), (311), (400), (511), and (440) for PVA@IONPs are low and wide, maybe due to the effect of disorder and a small crystallite. The peak extent depends on varied factors such as the strain effect and finite crystallite size. The Debye–Scherrer equation was used to calculate the size (Equation (1)). The calculated sizes for the PVA@IONPs and IONPs were 9.5 and 11.5 nm, respectively.

$$Dp = \frac{K\lambda}{\beta cos\theta} \quad (1)$$

where Dp is the grain size, β is the FWHM, λ is 1.5406 Å, K is the Scherrer constant, and θ is the Bragg angle.

The charges of the particles were investigated by zeta potential (ZP) measurements, which are an indicator of colloidal solution stability (Figure 3). The stability of the nanoparticle solution is significant for various applications so that expectable and proportionate outcomes can be obtained [31–37]. The IONPs (−2.49 mV) showed a lower ZP value than the PVA@IONPs (−10.59 mV). This reveals that IONPs may show low stability, where the lower ZP values will enhance Van der Waals attractions and allow highly aggregated particles. On the contrary, the higher ZP value of PVA@IONPs reveals that the particles may show high stability with a high electrostatic repulsive force [31]. A negative value of ZP was confirmed on the surface of magnetic PVA nanoparticles by Demerlis et al. The values showed that the nanoparticles displayed feasible colloidal stability concerning electrostatic repulsion [32]. In another report, a ZP value of -10.9 ± 3.5 mV was detected for PVA-layered Fe_3O_4 by Vilos et al. [33].

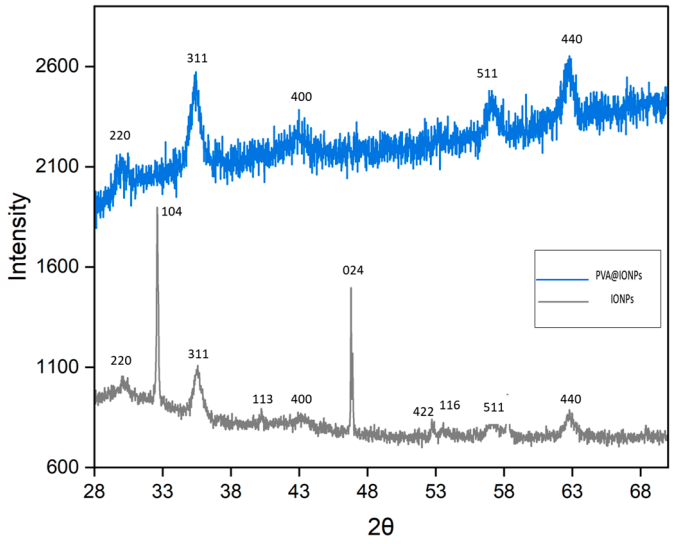

Figure 2. XRD of IONPs and PVA@IONPs.

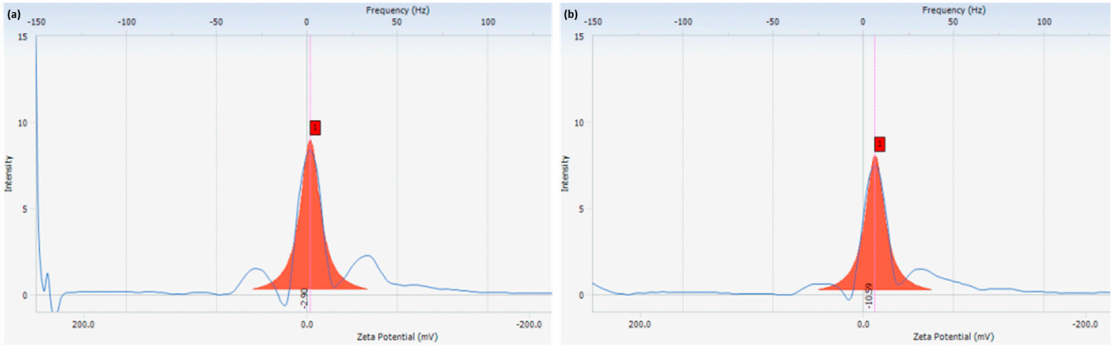

Figure 3. Zeta potential of (**a**) IONPs and (**b**) PVA@IONPs.

2.2. Magnetic Behavior of the Particles

A VSM was used to study the magnetic properties of the IONPs and PVA@IONPs at room temperature (RT) (Figure 4). The prepared magnetic nanoparticles showed soft magnetic properties with low remanence (Mr) and coercivity (Hc). The PVA@IONPs showed softening magnetic properties with a low coercivity of 7.8 G and remanence of 4.2 emu g^{-1}. When the size of magnetic nanoparticles is below the critical size within a nanoparticle fabrication, the magnetic nanoparticles like to act as a single magnetic domain structure. The smallest size shows super-paramagnetic properties under standard conditions. The magnetization (Ms) increases with the increase in the magnetic nanoparticle size to an extreme value near bulk magnetization. As the magnetic nanoparticles' size increases, they have pseudo-single domains and multi-domains, in which the moment of each domain is not aligned in the same direction. It was reported that a polyaniline shell/Fe_3O_4 showed a slight increase in Ms by 2 emu g^{-1} compared to naked Fe_3O_4 particles. This suggests that the small increase in the value of Ms may be due to the direct contact potential at the Fe_3O_4–polyaniline interface [34]. In another report, the same finding that the Ms of bare magnetite is less than for polymer-coated magnetite was detected by Mol et al. The Ms values of PANI-coated and polypyrrole-coated magnetite nanoparticles were 55 and 52 emu g^{-1}. The Ms value for magnetite was 51 emu g^{-1} less than for polymer-coated magnetite [35]. In our study, the values of Ms were 45.08 and 41.98 emu g^{-1} for the PVA@IONPs and IONPs (Figure 4). The small increase in the Ms value may be due to surface/interfacial magnetism. This noticed behavior agrees with the detection of a rise in the value of the Ms of polymer-coated magnetite [34,35].

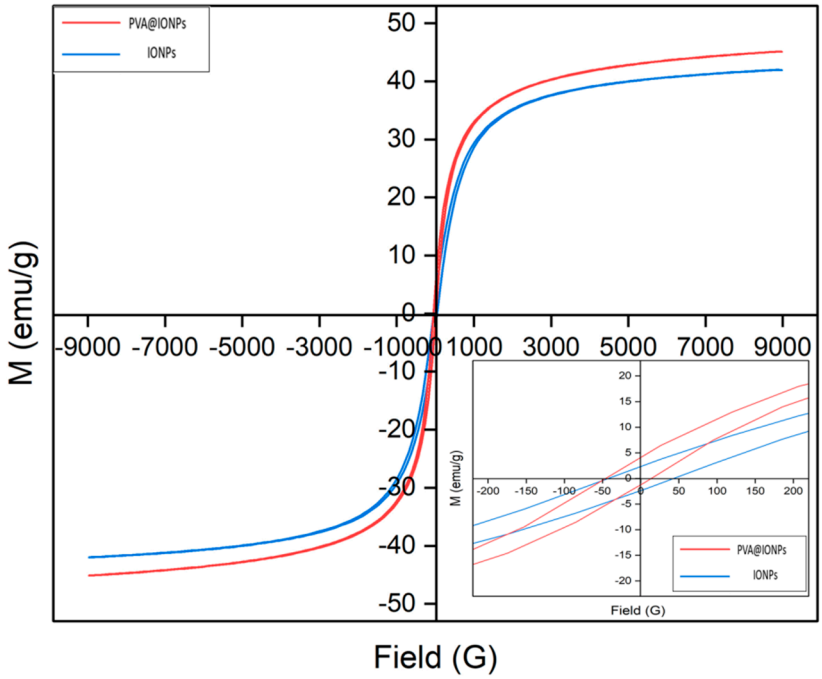

Figure 4. Magnetic properties of IONPs and PVA@IONPs.

2.3. Photoactivity of the Prepared Nanoparticles

The optical behaviors of the IONPs and PVA@IONPs were investigated via UV–Vis spectroscopy (Figure 5). The characteristic peaks for iron oxides are mostly within the wavelength range (nm) of 300–600 nm. The IONPs showed thermally promoted electronic transitions due to intervalence charge carriage. Absorbance of the magnetite phases in the fabricated magnetic material was observed. The magnetic nanoparticles exhibited absorption in the visible and near-IR regions [38]. Our magnetic nanoparticles showed a wide absorption spectrum in visible wavelengths ranging from 300 to 600 nm. The IONPs' peaks are located at 490 nm. On the other hand, the PVA@IONPs exhibit a shift in the absorption band and are located close together, with 494 nm corresponding to the d transition for Fe^{3+} [30].

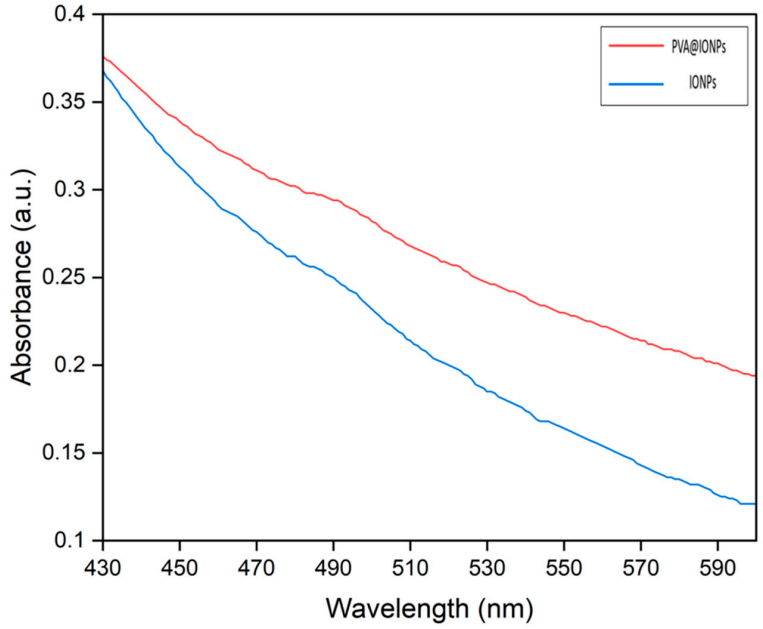

Figure 5. UV-Vis of IONPs and PVA@IONPs.

2.4. Hyperthermia Performance

Magnetic nanoparticles act as a thermal source and can produce localized heat energy under a magnetic field [39–46]. In Figure 6, the temperature increases with time almost in a linear path. Further, the rise in temperature slows down gradually to reach a saturation area where there is no change in the temperature, obtaining thermal equilibrium. Comparing the heating performance of the IONPs to the PVA@IONPs, the PVA@IONPs displayed the highest performance. Under the condition of a low magnetic field strength of 40 kA/m, it was obvious that the highest heating efficiency (10.9 °C) at 200 s was obtained for the PVA@IONPs. For the PVA@IONPs, the heating rate increased, and the temperature elevation was 13.5 °C at 200 s with the high magnetic field = 50 kA m^{-1}. For the IONPs, the temperature elevation was 7.2 °C at 200 s under the same magnetic field condition. Magnetic field energy can be converted into heat energy by magnetic nanoparticles via two relaxations, which are Neel and Brownian relaxations. In Brownian relaxation, heat is gained from the physical rotation of particles inside a medium, while in Neel relaxation, there is opposition from the particle's crystalline structure, resulting in heat generation. The improved stability, good dispersion, and rise in the value of Ms for PVA@IONPs enhance the self-heating effectively. The efficiency of induction heating depends on the nanoparticles' properties and magnetic field condition. IONPs have self-heating behavior, allowing their use in various applications including biomedical fields (hyperthermia and targeted drug delivery) as well as industrial fields (elastomer preparation) [47–58]. A magnetite poly(dimethylsiloxane) (PDMS) composite with improved thermal stability was fabricated under a magnetic field in a shorter time, making it a thermally stable elastomer [37]. In biomedical applications, magnetic iron oxide/polyvinyl alcohol/PMMA nanocomposites have been applied for ciprofloxacin delivery. The release of ciprofloxacin is increased under a magnetic field [52]. For effective self-heating performance, magnetic nanoparticles should have a small particle size with elevated magnetization saturation [53].

Table 1 shows a comparison between magnetic particles observed in the literature and the current study. The recorded values for the specific absorption rate (SAR) in the literature were 10–100 W g^{-1} for magnetic field conditions of H = 10 kA m^{-1} and f ≈ 400 kHz [43]. Magnetic nanoparticles with a size near 22 nm were the perfect size to improve the self-heating performance with super-paramagnetic properties [50]. The shape and particle size distribution were also remarkable factors associated with heating performance [51]. For biosafety, the AMF should be under a threshold safety value (5×10^9 A m^{-1} s^{-1}). So, our experimental conditions (3.8×10^9 and 4.8×10^9 $Am^{-1}s^{-1}$) for 40 and 50 kA/m, respectively, did not exceed the safety limit. The PVA@IONPs exhibited the highest specific absorption rate (SAR) with enhanced hyperthermic response. It was found that the PVA@IONPs (65.9 W g^{-1}) had a higher SAR value than the IONPs (55.6 W g^{-1}) under a frequency = 97 kHz and magnetic field = 50 kA m^{-1}. Tuning the shape, structure, and particle size of magnetic nanoparticles can switch their magnetic behavior, tune the Ms, and further improve self-heating efficiency.

Table 1. Comparison between magnetic particles observed in the literature and the current study.

Magnetic Particles	Coating Layer	Size (nm)	Ms (emu g^{-1})	SAR (W g^{-1})	Ref.
Fe_3O_4	PEG	19	80	2452	[43]
Fe_3O_4	Silica	10	3	20	[54]
Fe_3O_4	Silica	14.8	2.5	20	[55]
Fe_3O_4	-	7.5	10	15.5	[40]
Fe_3O_4	Chitosan	15.1 ± 5.0	49.96	118.85	[46]
Fe_3O_4	Citrate	10	76	171	[56]
Fe_3O_4	Dextran	5–15	49	36	[57]

Table 1. *Cont.*

Magnetic Particles	Coating Layer	Size (nm)	Ms (emu g^{-1})	SAR (W g^{-1})	Ref.
Fe_3O_4	-	10–12	41.98	55.6	Our study
Fe_3O_4	PVA	10–12	45.08	65.9	Our study

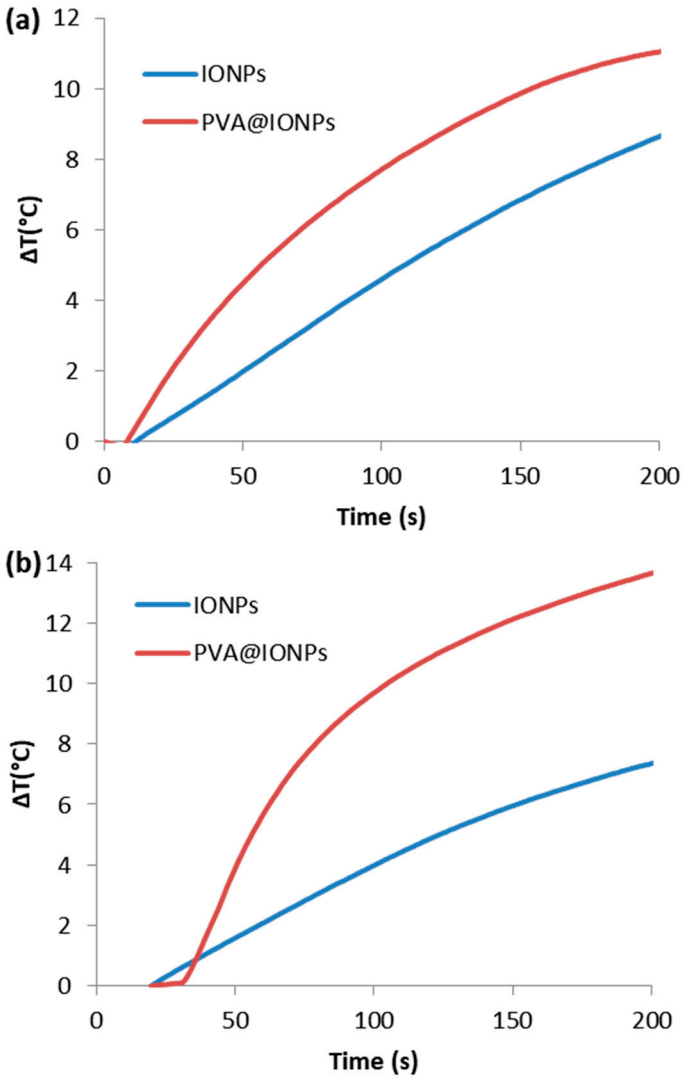

Figure 6. Heating curve of IONPs and PVA@IONPs under frequency = 97 kHz and magnetic fields of (**a**) 40 kA m^{-1} and (**b**) 50 kA m^{-1}.

2.5. Hydrogen Production Performance

The photocatalytic performances of the fabricated materials were studied for hydrogen production via water-splitting reactions. The performance was evaluated in terms of the shell structure, where the reaction was performed under the same conditions. Electrons were moved from the valence bands to the conduction bands after the fabricated photocatalysts adsorbed the energy. If the band gap is large enough and more than needed for the splitting reaction (1.23 eV), its band edge fits the thermodynamics required for the charge transfer. Then, the excited electron can reduce the hydrogen ions, and the holes can oxidize oxygen anions. Under visible light with magnetic force, the hydrogen performances were 60 and 127 mmole min^{-1} g^{-1} of photocatalysts for the IONPs and PVA@IONPs, respectively (Figure 7). The efficiency of IONPs as a photocatalyst in the water-splitting reaction could enhance the process. Hence, the presence of a shell layer could offer a key

part of the photocatalytic potential in the tuning of the produced gas's composition. In a hydrogen production system, a mixture solution of water and methanol is used. Through the photocatalytic reaction, the absorption of photons by the photocatalyst leads to the upgrading of an electron to conducting bands, thus creating e^-–h+ pairs. In such a reaction, a proton is generated due to water or methanol oxidation within the radiation-produced holes. Protons were then engaged in the reduction system, by electrons, at the surface of the photocatalyst to produce hydrogen, as illustrated in Equations [59–70].

$$hv \rightarrow e^- + hole^+$$

$$4hole^+ + 2H_2O \rightarrow 2O + 4H^+$$

$$2H^+ + 2e^- \rightarrow H_2$$

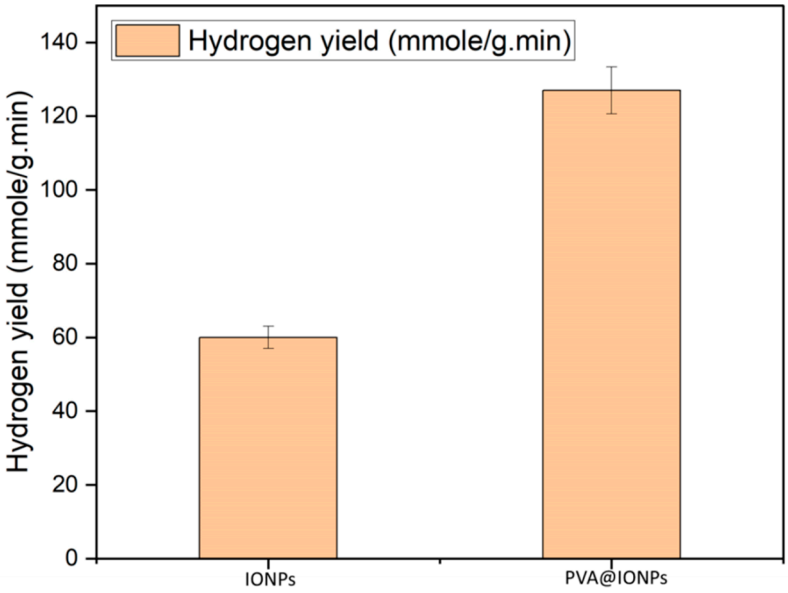

Figure 7. Hydrogen yields of IONPs and PVA@IONPs.

Methanol is used to prohibit the revealing of oxygen gas that may occur due to water adsorption on the surface of the catalyst. Methanol has been employed to hinder the reaction of the regrouping hole–electron pairs. Also, methanol acts as a hole scavenger. Methanol could take part in hydrogen production, as illustrated in Equations [60].

$$MeOH \leftrightarrow H_2 + H_2CO$$

$$O_2 + H_2CO \leftrightarrow H_2CO_2$$

$$H_2CO_2 \leftrightarrow CO_2 + H_2$$

PVA with dense electrons of free lone pairs could strongly affect the photobehavior by absorbing light irradiation and instantly being excited by the influence of irradiation. The excited electron could, on the one hand, interfere with the metal oxide electrons and reduce the band gap. Higher-magnetization PVA@IONPs could also enhance the photocatalytic performance by decreasing light irradiation scattering during the process. The hydrogen performance for the PVA@IONPs was more than twofold that of the core IONPs. The production of hydrogen using water, a catalyst, and solar energy is one of the extreme potential outlets for clean energy generation. PVA@IONPs display superior photocatalytic activity for hydrogen production against IONPs, with promising performance in a water-splitting system.

Table 2 shows a comparison between hydrogen yields observed in the literature and the current study. An enhancement in hydrogen yield could be achieved by the magnetic property through splitting via magnetic force. Therefore, scattered radiation could be reduced during the splitting process. So, the magnetic property could result in the spin polarization of electronic systems of photocatalysts due to the presence of the magnetic force [61]. The existence of an external magnetic field can improve the photocatalytic reaction by increasing carrier transport and decreasing recombination [59,60]. It was found that a magnetic field could hinder the photo-induced charge recombination of zinc ferrite ($ZnFe_2O_4$), as the polarization could be controlled via magnetic fields, enhancing the photoelectron chemical performance [55]. A magnetic field was believed to assist the photocatalytic reaction by creating the separation of photo-generated charges [64,65]. The electron's spin polarization could enhance the movement of the photocatalyst particles through the reaction. Hence, improved interactions between the particles and the water molecules occurred. Spin polarization, magneto-resistance, and Lorentz force can hinder photo-generated electron–hole recombination and increase carrier transfer performance. Although using an external magnetic field gives outstanding improved results in photocatalytic systems, the enhancement mechanism of the magnetic field on the photocatalytic system still needs to be further investigated. The presence of a magnetic field can improve the photocatalytic performance, but the mechanism of magnetic field-promoted photo-generated electron transfer in catalysts is still relatively ambiguous, and a clear quantitative relationship between them cannot not be determined. Therefore, it is necessary to explore more techniques, especially time-resolved techniques, superconducting quantum interference devices, and electron paramagnetic resonance, all of which can provide a clearer and more precise understanding of the mechanisms behind magnetic field enhancement [9].

Table 2. Comparison between hydrogen yields observed in the literature and the current study.

Materials	Hydrogen Yield (μmol $h^{-1}g^{-1}$)	Ref.
PEI-Ag@Fe_2O_3	540,000	[61]
(CdS + ZnS)/Fe_2O_3	4129	[66]
TiO_2/Fe_2O_3	2700	[67]
$Zn_{0.8}Cd_{0.2}S$@g-C_3N_4	2351.18	[68]
Fe_3O_4@ZnS	3900	[69]
Fe_3O_4	1000	Our study
PVA@Fe_3O_4	2116	Our study

3. Materials and Methods

3.1. Materials

Iron (III) chloride hexahydrate, iron (II) chloride tetrahydrate, polyvinyl alcohol (Mw 30–70 kDa), and ammonium hydroxide (30% NH_3 in H_2O) were ordered from Sigma Aldrich (St. Louis, MO, USA).

3.2. Preparation of Magnetic Materials

3.2.1. Synthesis of Iron Oxide Nanoparticles (IONPs)

Ferric chloride hexahydrate (5.4 g, 0.009 mole) and ferrous chloride tetrahydrate (1.9 g, 0.019 mole) were dissolved in distilled water (DW, 150 mL). The solution was mixed well with a stirrer for 30 min, and then the temperature was raised to 70 °C. The calculated amount of ammonium hydroxide (6 mL, 6.6 mole) was added to produce a precipitate of iron oxide nanoparticles (IONPs). The IONPs were separated using a magnetic bar and washed many times with DW, then finally dried until a powder was obtained.

3.2.2. Synthesis of Polymeric Polyvinyl Alcohol–Stabilized Iron Oxide Nanoparticles (PVA@IONPs)

The calculated amount of polyvinyl alcohol (0.5 g, 0.0071 mmole) was dissolved in 50 mL of DW. Sonication of the mixture was performed at room temperature using a US bath (28 kHz) for 30 min to obtain a homogenous solution. Then, the prepared iron oxide nanoparticles (1.5 g) were solubilized in the solution and sonicated (28 kHz) for an additional 60 min at room temperature. Separation of the polymeric polyvinyl alcohol–stabilized iron oxide nanoparticles (PVA@IONPs) using a magnetic bar was performed; then, they were washed many times with DW and finally dried until a powder was obtained.

3.3. Hyperthermia Performance of the Fabricated Magnetic Nanoparticles

The self-heating performance of the fabricated nanoparticles was evaluated based on the value of specific absorption rate (SAR) (Equation (2)). The SAR value was estimated under a magnetic field (H = 40 and 50 kA m^{-1}) and frequency (f = 97 kHz).

$$SAR = (Cp/m) \times (dT/dt) \quad (2)$$

where dT/dt (temperature with time), Cp (4.184 J/g °C), and m (Fe weight).

3.4. Photocatalytic Performance of the Fabricated Nanoparticles

As described in our previous research, the catalysts (0.5 g) were added to a methanol/water solution. The system was degassed and subjected to the vis. light spectrum (intensity of 0.13 W/mL) at ambient temperature and under magnetic force for 45 min. The obtained gas was investigated via gas chromatography (GC). Hydrogen production experiments were conducted in triplicate to confirm the uniformity of the obtained results.

3.5. Characterizations

XRD was investigated via an X-ray diffractometer (Rigaku, Tokyo, Japan). Zeta potential measurements were obtained using a zeta potential and particle size analyzer (ELSZ-2000; Photal Otsuka Electronics, Osaka, Japan). UV spectroscopic analysis was performed via a UV spectrophotometer (V-570, JASCO, Tokyo, Japan). The magnetic property was studied via a VSM (Lake Shore 7400 series; Lake Shore Cryotronics, Westerville, OH, USA). The metal contents were calculated via an ICP-OES (Optima 8300, PerkinElmer, Waltham, MA, USA). The morphology was studied using TEM (JEM-2100 LaB6, JEOL, Akishima, Tokyo, Japan) at 200 keV.

4. Conclusions

Polymeric PVA@IONPs were produced successfully via an ultrasonic-assisted coprecipitation process by the solution-mixing technique at room temperature. The zeta potential value for the PVA@IONPs was −10.59 mV, implying that the prepared particles may display good stability in water. The presence of a PVA shell on the surface of the IONPs led to an improved mono-dispersion property. The PVA layer enhanced the advantage of increasing the repulsion to balance the magnetic and Van der Waals forces. The prepared PVA@IONPs had an almost spherical shape with a mean size of 16 nm. They showed high saturation magnetization with low coercivity at 45 emu g^{-1} and 7.8 G, respectively. The hydrogen yield was 127 mmole min^{-1} g^{-1} for the PVA@IONPs under visible light with magnetic force. The PVA@IONPs (65.9 W g^{-1}) exhibited a higher specific absorption rate than the IONPs (55.6 W g^{-1}) with good self-heating performance. The PVA@IONPs showed outstanding self-heating and photocatalytic performances when used as promising magnetic tuning stimuli-responsive polymeric nanoparticles for varied applications.

Author Contributions: Conceptualization, resources, supervision, writing—review and editing. M.M.K.; conceptualization, resources, supervision, writing—review and editing, H.A.; conceptualization, methodology, writing—original draft, M.S.A.D. All authors have read and agreed to the published version of the manuscript.

Funding: This research was funded by Deputyship for Research & Innovation, Ministry of Education in Saudi Arabia, project number IFP22UQU4290670DSR163.

Data Availability Statement: Data are contained within the article.

Acknowledgments: The authors extend their appreciation to the Deputyship for Research & Innovation, Ministry of Education in Saudi Arabia, for funding this research work through project number IFP22UQU4290670DSR163.

Conflicts of Interest: The authors declare no conflicts of interest.

References

1. Vera, M.; Mella, C.; Urbano, B.F. Smart polymer nanocomposites: Recent advances and perspectives. *J. Chil. Chem. Soc.* **2020**, *65*, 4973–4981. [CrossRef]
2. Talaat, A.; Suraj, M.V.; Byerly, K.; Wang, A.; Wang, Y.; Lee, J.K.P.; Ohodnicki, R., Jr. Review on soft magnetic metal and inorganic oxide nanocomposites for power applications. *J. Alloys Compd.* **2021**, *870*, 159500. [CrossRef]
3. Darwish, M.S.A.; Mostafa, M.H.; Al-Harbi, L.M. Polymeric Nanocomposites for Environmental and Industrial Applications. *Int. J. Mol. Sci.* **2022**, *23*, 1023. [CrossRef] [PubMed]
4. Wu, H.; Fahy, W.P.; Kim, S.; Kim, H.; Zhao, N.; Pilato, L.; Kafi, A.; Bateman, S.; Koo, J.H. Recent developments in polymers/polymer nanocomposites for additive manufacturing. *Prog. Mater. Sci.* **2020**, *111*, 100638. [CrossRef]
5. Mukhopadhyay, R.; Bhaduri, D.; Sarkar, B.; Rusmin, R.; Hou, D.; Khanam, R.; Sarkar, S.; Biswas, J.K.; Vithanage, M.; Bhatnagar, A. Clay–polymer nanocomposites: Progress and challenges for use in sustainable water treatment. *J. Hazard. Mater.* **2020**, *383*, 121125. [CrossRef] [PubMed]
6. Jamróz, E.; Kulawik, P.; Kopel, P. The effect of nanofillers on the functional properties of biopolymer-based films: A review. *Polymers* **2019**, *11*, 675. [CrossRef] [PubMed]
7. Mout, R.; Moyano, D.F.; Rana, S.; Rotello, V.M. Surface functionalization of nanoparticles for nanomedicine. *Chem. Soc. Rev.* **2012**, *41*, 2539–2544. [CrossRef] [PubMed]
8. Jawed, A.; Saxena, V.; Pandey, L.M. Engineered nanomaterials and their surface functionalization for the removal of heavy metals: A review. *J. Water Process Eng.* **2020**, *33*, 101009. [CrossRef]
9. Meng, S.; Li, Y.; Liu, Y.; Zhan, S.; Ma, Q.; Li, Y. Recent advances and mechanisms in magnetic field enhanced photocatalysis: A review. *Environ. Surf. Interfaces* **2023**, *1*, 10–23. [CrossRef]
10. Yang, H.; Wang, F.; Zhang, H.; Guo, L.; Hu, L.; Wang, L.; Xue, D.J.; Xu, X. Solution Synthesis of Layered van der Waals (vdW) Ferromagnetic $CrGeTe_3$ Nanosheets from a Non-vdW Cr_2Te_3Template. *J. Am. Chem. Soc.* **2020**, *142*, 4438–4444. [CrossRef]
11. Yan, Y.; Lin, J.; Xu, T.; Liu, B.; Huang, K.; Qiao, L.; Liu, S.; Cao, J.; Jun, S.C.; Yamauchi, Y.; et al. Atomic-Level Platinum Filling into Ni-Vacancies of Dual-Deficient NiO for Boosting Electrocatalytic Hydrogen Evolution. *Adv. Energy Mater.* **2022**, *12*, 2200434. [CrossRef]
12. Yan, Y.; Lin, J.; Huang, K.; Zheng, X.; Qiao, L.; Liu, S.; Cao, J.; Jun, S.C.; Yamauchi, Y.; Qi, J. Tensile Strain-Mediated Spinel Ferrites Enable Superior Oxygen Evolution Activity. *J. Am. Chem. Soc.* **2023**, *145*, 24218–24229. [CrossRef]
13. Ganguly, S.; Margel, S. 3D printed magnetic polymer composite hydrogels for hyperthermia and magnetic field driven structural manipulation. *Prog. Polym. Sci.* **2022**, *131*, 101574. [CrossRef]
14. Ganguly, S.; Margel, S. Design of magnetic hydrogels for hyperthermia and drug delivery. *Polymers* **2021**, *13*, 4259. [CrossRef]
15. Biswas, A.; Patra, A.K.; Sarkar, S.; Das, D.; Chattopadhyay, D.; De, S. Synthesis of highly magnetic iron oxide nanomaterials from waste iron by one-step approach. *Colloids Surf. A Physicochem. Eng. Asp.* **2020**, *589*, 124420. [CrossRef]
16. Maity, D.; Mollick, M.R.; Mondal, D.; Bhowmick, B.; Neogi, S.K.; Banerjee, A.; Chattopadhyay, S.; Bandyopadhyay, S.; Chattopadhyay, D. Synthesis of HPMC stabilized nickel nanoparticles and investigation of their magnetic and catalytic properties. *Carbohydr. Polym.* **2013**, *98*, 80–88. [CrossRef] [PubMed]
17. Wanna, Y.; Chindaduang, A.; Tumcharern, G.; Phromyothin, D.; Porntheerapat, S.; Nukeaw, J.; Hofmann, H.; Pratontep, S. Efficiency of SPIONs functionalized with polyethylene glycol bis (amine) for heavy metal remova. *J. Magn. Magn. Mater.* **2016**, *414*, 32–37. [CrossRef]
18. Qiu, X.P.; Winnik, F. Preparation and characterization of PVA coated magnetic nanoparticles. *Chin. J. Polym. Sci.* **2000**, *18*, 535–539.
19. Maleki, A.; Rahimi, J.; Hajizadeh, Z.; Niksefat, M. Synthesis and characterization of an acidic nanostructure based on magnetic polyvinyl alcohol as an efficient heterogeneous nanocatalyst for the synthesis of a-aminonitriles. *J. Organomet. Chem.* **2019**, *881*, 58–65. [CrossRef]
20. Wei, Y.; Zhang, X.; Song, Y.; Han, B.; Hu, X.; Wang, X.; Lin, Y.; Deng, X. Magnetic biodegradable Fe3O4/CS/PVA nanofibrous membranes for bone regeneration. *Biomed Mater.* **2011**, *6*, 55008. [CrossRef]
21. Zélis, P.M.; Muraca, D.; Gonzalez, J.S. Magnetic properties study of iron-oxide nanoparticles/PVA ferrogels with potential biomedical applications. *J. Nanopart. Res.* **2013**, *15*, 1613. [CrossRef]
22. Saghafi, M.; Hosseini, S.A.; Zangeneh, S.; Moghanian, A.H.; Salarvand, V.; Vahedi, S.; Mohajerzadeh, S. Charge storage properties of mixed ternary transition metal ferrites MZnFe oxides (M 14 Al, Mg, Cu, Fe, Ni) prepared by hydrothermal method. *SN Appl. Sci.* **2019**, *1*, 1303. [CrossRef]

23. Ye, Y.; Al-Khaledi, N.; Barker, L.; Darwish, M.S.; El Naggar, A.M.; El-Yahyaoui, A.; Hussein, A.; Hussein, E.S.; Shang, D.; Taha, M.; et al. Uranium resources in China's phosphate rocks—Identifying low-hanging fruits. *IOP Conf. Ser. Earth Environ. Sci.* **2019**, *227*, 052033. [CrossRef]
24. Motawie, M.; Hanafi, S.A.; Elmelawy, M.S.; Ahmed, S.M.; Mansour, N.A.; Darwish, M.S.; Abulyazied, D.E. Wax co-cracking synergism of high density polyethylene to alternative fuels. *Egypt. J. Pet.* **2015**, *24*, 353–361. [CrossRef]
25. Darwish, M.S.A.; Kunz, U.; Peuker, U. Preparation and catalytic use of platinum in magnetic core/shell nanocomposites. *J. Appl. Polym. Sci.* **2013**, *129*, 1806–1811. [CrossRef]
26. Bhagwat, V.R.; Humbe, A.V.; More, S.D.; Jadhav, K.M. Sol-gel auto combustion synthesis and characterizations of cobalt ferrite nanoparticles: Different fuels approach. *Mater. Sci. Eng. B* **2019**, *248*, 114388. [CrossRef]
27. Darwish, M.S.A.; El-Sabbagh, A.; Stibor, I. Hyperthermia properties of magnetic polyethylenimine core/shell nanoparticles: Influence of carrier and magnetic strength. *J. Polym. Res.* **2015**, *22*, 239. [CrossRef]
28. Bhardwaj, A.; Jain, N.; Parekh, K. Investigating the effect of outer layer of magnetic particles on cervical cancer cells HeLa by magnetic fuid hyperthermia. *Cancer Nano* **2021**, *12*, 7. [CrossRef]
29. Anbarasu, M.; Anandan, M.; Chinnasamy, E.; Gopinath, V.; Balamurugan, K. Synthesis and characterization of polyethylene glycol (PEG) coated Fe3O4 nanoparticles by chemical co-precipitation method for biomedical applications. *Spectrochim. Acta A* **2015**, *135*, 536–539. [CrossRef]
30. Sarkar, A.; Biswas, S.K.; Pramanik, P. Design of a new nanostructure comprising mesoporous ZrO_2 shell and magnetite core (Fe_3O_4@mZrO_2) and study of its phosphate ion separation efficiency. *J. Mater. Chem.* **2010**, *20*, 4417–4424. [CrossRef]
31. Kmita, A.; Lachowicz, D.; Żukrowski, J.; Gajewska, M.; Szczerba, W.; Kuciakowski, J.; Zapotoczny, S.; Sikora, M. One-step synthe sis of long term stable superparamagnetic colloid of zinc ferrite nanorods in water. *Materials* **2019**, *12*, 1048. [CrossRef] [PubMed]
32. Demerlis, C.C.; Schoneker, D.R. Review of the oral toxicity of poly vinyl alcohol (PVA). *Food Chem. Toxicol.* **2003**, *41*, 319–326. [CrossRef] [PubMed]
33. Vilos, C.; Gutierrez, M.; Escobar, R.; Morales, F.; Denardin, J.; Velásquez, L.; Altbir, D. Superparamagnetic poly (3-hydroxybu tyrate-co-3 hydroxyvalerate) (PHBV) nanoparticles for biomedical applications. *Electron. J. Biotechnol.* **2013**, *16*, 5. [CrossRef]
34. Sethulakshmi, N.; Sooraj, V.; Sajeev, U.S.; Nair, S.S.; Narayanan, T.N.; Joy, L.K.; Joy, P.A.; Ajayan, P.M.; Anantharaman, M.R. Contact potential induced enhancement of magnetization in polyaniline coated nanomagnetic iron oxides by plasma polymerization. *Appl. Phys. Lett.* **2013**, *103*, 162414. [CrossRef]
35. Mol, B.; Beeran, A.E.; Jayaram, P.S.; Prakash, P.; Jayasree, R.S.; Thomas, S.; Chakrapani, B.; Anantharaman, M.R.; Bushiri, M.J. Radio frequency plasma assisted surface modifcation of Fe_3O_4 nanoparticles using polyaniline/polypyrrole for bioimaging and magnetic hyperthermia applications. *J. Mater. Sci. Mater. Med.* **2021**, *32*, 108. [CrossRef] [PubMed]
36. Kurchania, R.; Sawant, S.S.; Ball, R.J. Synthesis and characterization of magnetite/polyvinyl alcohol core-shell composite nanoparticles. *J. Am. Ceram. Soc.* **2014**, *97*, 3208–3215. [CrossRef]
37. Kayal, S.; Ramanujan, R.V. Doxorubicin loaded PVA coated iron oxide nanoparticles for targeted drug delivery. *Mater. Sci. Eng. C Biom. Mater. Sens. Syst.* **2010**, *30*, 484–490. [CrossRef]
38. Badawy, S.M.; Abd, E.-L. Synthesis and characterizations of magnet ite nanocomposite films for radiation shielding. *Polym. Compos.* **2017**, *38*, 974–980. [CrossRef]
39. Piñeiro-Redondo, Y.; Bañobre-López, M.; Pardiñas-Blanco, I.; Goya, G.; López-Quintela, M.A.; Rivas, J. The influence of colloidal parameters on the specific power absorption of PAA-coated magnetite nanoparticles. *Nanoscale Res. Lett.* **2011**, *6*, 383. [CrossRef]
40. Ma, M.; Wu, Y.; Zhou, J.; Sun, Y.; Zhang, Y.; Gu, N. Size dependence of specific power absorption of Fe_3O_4 particles in AC magnetic field. *J. Magn. Magn. Mater.* **2004**, *268*, 33–39. [CrossRef]
41. Hergt, R.; Hiergeist, R.; Zeisberger, M.; Glockl, G.; Weitschies, W.; Ramirez, L.P.; Hilger, I.; Kaiser, W.A. Enhancement of AC-losses of magnetic nanoparticles for heating applications. *J. Magn. Magn. Mater.* **2004**, *80*, 358–368. [CrossRef]
42. Hergt, R.; Dutz, S. Magnetic particle hyperthermia—Biophysical limitations of a visionary tumour therapy. *J. Magn. Magn. Mater.* **2007**, *311*, 187–192. [CrossRef]
43. Hergt, R.; Dutz, S.; Muller, R.; Zeisberger, M. Magnetic particle hyperthermia: Nanoparticle magnetism and materials develop ment for cancer therapy. *J. Phys. Condens. Matter.* **2006**, *18*, S2919. [CrossRef]
44. Nigam, S.; Barick, K.; Bahadur, D. Development of citrate-stabilized Fe_3O_4 nanoparticles: Conjugation and release of doxorubicin for therapeutic applications. *J. Magn. Magn. Mater.* **2011**, *323*, 237–243. [CrossRef]
45. Reyes-Ortega, F.; Delgado, Á.V.; Schneider, E.K.; Checa Fernández, B.L.; Iglesias, G.R. Magnetic nanoparticles coated with a thermosensitive polymer with hyperthermia properties. *Polymers* **2018**, *10*, 10. [CrossRef] [PubMed]
46. Shete, P.B.; Patil, R.M.; Thorat, N.D.; Prasad, A.; Ningthoujam, R.S.; Ghosh, S.J.; Pawar, S.H. Magnetic chitosan nanocomposite for hyperthermia therapy application: Preparation, characterization and in vitro experiments. *Appl. Surf. Sci.* **2014**, *288*, 149–157. [CrossRef]
47. Darwish, M.S.A.; Stibor, I. Preparation and characterization of magnetite–PDMS composites by magnetic 1053 induction heating. *Mater. Chem. Phys.* **2015**, *164*, 163–169. [CrossRef]
48. Li, J.; Zheng, L.; Cai, H.; Sun, W.; Shen, M.; Zhang, G.; Shi, X. Polyethyleneimine-mediated synthesis of folic acid-targeted iron oxide nanoparticles for in vivo tumor MR imaging. *Biomaterials* **2013**, *34*, 8382–8392. [CrossRef]
49. Nitin, N.; LaConte, L.E.W.; Zurkiya, O.; Hu, X.; Bao, G. Functionalization and peptide-based delivery of magnetic nanoparticles as an intracellular MRI contrast agent. *J. Biol. Inorg. Chem.* **2004**, *9*, 706–712. [CrossRef]

50. Rosensweig, R.E. Heating Magnetic Fluid with Alternating Magnetic Field. *J. Magn. Magn. Mater.* **2002**, *252*, 370. [CrossRef]
51. Noh, S.H.; Na, W.; Jang, J.T.; Lee, J.H.; Lee, E.J.; Moon, S.H.; Lim, Y.; Shin, J.S.; Cheon, J. Nanoscale magnetism control via surface and exchange anisotropy for optimized ferrimagnetic hysteresis. *Nano Lett.* **2012**, *12*, 3716. [CrossRef] [PubMed]
52. Bajpai, A.K.; Gupta, R. Magnetically mediated release of ciprofloxacin from polyvinyl alcohol based superparamagnetic nanocomposites. *J. Mater. Sci. Mater. Med.* **2011**, *22*, 357–369. [CrossRef] [PubMed]
53. Guardia, P.; Di Corato, R.; Lartigue, L.; Wilhelm, C.; Espinosa, A.; Garcia-Hernandez, M.; Gazeau, F.; Manna, L.; Pellegrino, T. Water-soluble iron oxide nanocubes with high values of specific absorption rate for cancer cell hyperthermia treatment. *ACS Nano* **2012**, *6*, 3080–3091. [CrossRef]
54. Le Renard, P.E.; Lortz, R.; Senatore, C.; Rapin, J.P.; Buchegger, F.; Petri-Fink, A.; Hofmann, H.; Doelker, E.; Jordan, O. Magnetic and in vitro heating properties of implants formed in situ from injectable formulations and containing superparamagnetic iron oxide nanoparticles (SPIONs) embedded in silica microparticles for magnetically induced local hyperthermia. *J. Magn. Magn. Mater.* **2011**, *323*, 1054–1063. [CrossRef]
55. Owens, F. Ferromagnetic resonance observation of a phase transition in magnetic field-aligned Fe_2O_3 nanoparticles. *J. Magn. Magn. Mater.* **2009**, *321*, 2386–2391. [CrossRef]
56. Vassallo, M.; Martella, D.; Barrera, G.; Celegato, F.; Coïsson, M.; Ferrero, R.; Olivetti, E.S.; Troia, A.; Sözeri, H.; Parmeggiani, C.; et al. Improvement of Hyperthermia Properties of Iron Oxide Nanoparticles by Surface Coating. *ACS Omega* **2023**, *8*, 2143–2154. [CrossRef] [PubMed]
57. El-Boubbou, K.; Lemine, O.M.; Ali, R.; Huwaizi, S.M.; Al-Humaid, S.; AlKushi, A. Evaluating magnetic and thermal effects of various Polymerylated magnetic iron oxide nanoparticles for combined chemo-hyperthermia. *New J. Chem.* **2022**, *46*, 5489–5504. [CrossRef]
58. Nisticò, R.; Cesano, F.; Garello, F. Magnetic Materials and Systems: Domain Structure Visualization and Other Characterization Techniques for the Application in the Materials Science and Biomedicine. *Inorganics* **2020**, *8*, 6. [CrossRef]
59. Choi, H.-J.; Kang, M. Hydrogen production from methanol–water decomposition in a liquid photosystem using the anatase structure of Cu loaded TiO_2. *Int. J. Hydrog. Energy* **2007**, *32*, 3841–3848. [CrossRef]
60. Chen, J.; Ollis, D.F.; Rulken, W.H.; Bruning, H. Photocatalyzed oxidation of alcohols and organochlorides in the presence of nativeTiO_2 and metallized TiO_2 suspensions. Part (II): Photocatalytic mechanisms. *Water Res.* **1999**, *33*, 669–676. [CrossRef]
61. Darwish, M.S.; El Naggar, A.M.; Morshedy, A.S.; Haneklaus, N. Increased production of hydrogen with in situ CO_2 capture through the process of water splitting using magnetic core/shell structures as novel photocatalysts. *Environ. Sci. Pollut. Res.* **2021**, *28*, 3566–3578. [CrossRef] [PubMed]
62. Huang, H.J.; Wang, Y.H.; Chau, Y.F.C.; Chiang, H.P.; Wu, J.C.S. Magnetic Field-Enhancing Photocatalytic Reaction in Micro Optofluidic Chip Reactor. *Nanoscale Res. Lett.* **2019**, *14*, 323. [CrossRef] [PubMed]
63. Gao, W.; Peng, R.; Yang, Y.; Zhao, X.; Cui, C.; Su, X.; Qin, W.; Dai, Y.; Ma, Y.; Liu, H.; et al. Electron Spin Polarization-Enhanced Photoinduced Charge Separation in Ferromagnetic $ZnFe_2O_4$. *ACS Energy Lett.* **2021**, *6*, 2129–2137. [CrossRef]
64. Li, J.; Pei, Q.; Wang, R.Y.; Zhou, Y.; Zhang, Z.M.; Cao, Q.Q.; Wang, D.H.; Mi, W.B.; Du, Y.W. Enhanced photocatalytic performance through magnetic field boosting carrier transport. *ACS Nano* **2018**, *12*, 3351–3359. [CrossRef] [PubMed]
65. Li, J.; Yin, W.; Pan, J.; Zhang, Y.; Wang, F.; Wang, L.; Zhao, Q. External field assisted hydrogen evolution reaction. *Nano Res.* **2023**, *16*, 8638–8654. [CrossRef]
66. Preethi, V.; Kanmani, S. Photocatalytic hydrogen production using Fe_2O_3-based core shell nano particles with ZnS and CdS. *Int. J. Hydrog. Energy* **2014**, *39*, 1613–1622. [CrossRef]
67. Madhumitha, A.; Preethi, V.; Kanmani, S. Photocatalytic hydrogen production using TiO_2 coated iron-oxide core shell particles. *Int. J. Hydrog. Energy* **2018**, *43*, 3946–3956. [CrossRef]
68. Tian, F.-Y.; Hou, D.; Tang, F.; Deng, M.X.-Q.; Zhang, Q.; Wu, T.; Li, D.-S. Novel $Zn_{0.8}Cd_{0.2}S$@g-C_3N_4 core–shell heterojunctions with a twin structure for enhanced visible-light-driven photocatalytic hydrogen generation. *J. Mater. Chem. A* **2018**, *6*, 17086–17094. [CrossRef]
69. Chang, C.-J.; Lee, Z.; Wei, M.D.; Chang, C.-C.; Chu, K.-W. Photocatalytic hydrogen production by magnetically separable Fe_3O_4@ZnS and $NiCo_2O_4$@ZnS core-shell nanoparticles. *Int. J. Hydrog. Energy* **2015**, *40*, 11436–11443. [CrossRef]
70. Alharthi, F.A.; Ababtain, A.S.; Alanazi, H.S.; Al-Nafaei, W.S.; Hasan, I. Synthesis of $Zn_3V_2O_8$/rGO Nanocomposite for Photocatalytic Hydrogen Production. *Inorganics* **2023**, *11*, 93. [CrossRef]